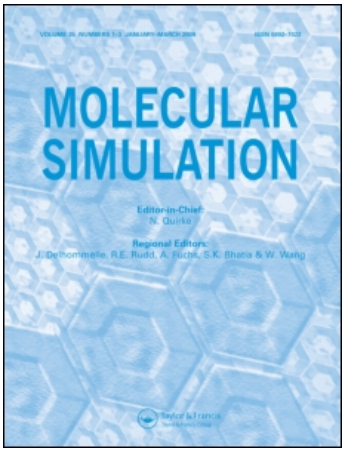

Molecular Simulation
Publication details, including instructions for authors and subscription information:
http://www.informaworld.com/smpp/title~content=t713644482

Mechanical properties and electronic structures of compressed C_{60}, $C_{60}F_{60}$ and $C_{60}H_{60}$ molecules

Haijun Shen[a]
[a] School of Aerospace Engineering & Applied Mechanics, Tongji University, Shanghai, People's Republic of China

To cite this Article Shen, Haijun(2009) 'Mechanical properties and electronic structures of compressed C_{60}, $C_{60}F_{60}$ and $C_{60}H_{60}$ molecules', Molecular Simulation, 35: 3, 193 — 198
To link to this Article: DOI: 10.1080/08927020802430737
URL: http://dx.doi.org/10.1080/08927020802430737

Molecular Simulation
Vol. 35, No. 3, March 2009, 193–198

Taylor & Francis
Taylor & Francis Group

Mechanical properties and electronic structures of compressed C_{60}, $C_{60}F_{60}$ and $C_{60}H_{60}$ molecules

Haijun Shen*

School of Aerospace Engineering & Applied Mechanics, Tongji University, Shanghai 200092, People's Republic of China

(*Received 4 December 2007; final version received 25 August 2008*)

By using the quantum molecular dynamics technique, the compression of C_{60}, $C_{60}F_{60}$ and $C_{60}H_{60}$ molecules was simulated, and their electronic structures under compression were calculated. According to the obtained results, the compressive mechanical properties of the three molecules, as well as the effects of compressive deformation on their electronic structures, were discussed. It is shown that (1) the load support and energy-absorbing capabilities of the three molecules both have the order of $C_{60}F_{60} > C_{60}H_{60} > C_{60}$, but their deformation support capability is comparable, and (2) with the increase of compressive strain, the three molecules become more chemically active, but under the same compressive strain, the $C_{60}F_{60}$ and $C_{60}H_{60}$ molecules have better chemical stability than the C_{60} molecule.

Keywords: C_{60}; $C_{60}F_{60}$; $C_{60}H_{60}$; compressive properties; electronic structures

1. Introduction

In recent years, experimental scientists have obtained a number of cage-like carbon molecules. The molecules are called carbon fullerenes and include C_{24}, C_{36}, C_{60}, C_{70}, C_{80}, C_{240} and so on [1,2]. The analysis of time-of-flight mass spectra indicates that among the carbon molecules C_{60} is dominant and most chemically stable [3]. C_{60} fullerene has spherical molecular configuration and 60 atoms distributed on its surface. Because of its stability and spherical symmetry, C_{60} has been considered as a potential molecular lubricant for microelectromechanical systems (MEMS) and nanoelectromechanical systems (NEMS) [4–6].

Since the discovery and large-scale preparation of C_{60}, the chemistry of fullerenes has become one of the most developing fields in organic chemistry [7]. Recently, the fully fluorinated and hydrogenated C_{60} molecules, i.e. $C_{60}F_{60}$ and $C_{60}H_{60}$, have been reported [8]. The molecules are predicted to be attainable through adding H or F atoms to the outside of C_{60} fullerene [9], which would cause $C_{60}F_{60}$ and $C_{60}H_{60}$ to take on a fuzzy appearance (Figure 1(b)), hence the name fuzzy ball [10]. The theoretical results of [6] show that the fuzzy balls of $C_{60}H_{60}$ or $C_{60}F_{60}$ have wider lowest unoccupied molecular orbital (LUMO)–highest occupied molecular orbital (HOMO) energy gap, i.e. better chemical stability, and are likely to create a slicker molecular lubricant than C_{60}.

Considering that under the action of friction pairs in MEMS and NEMS, compressive deformation will occur in the molecular 'bearing balls' of C_{60}, $C_{60}F_{60}$ and $C_{60}H_{60}$, and the deformed molecules always tend to become more chemically active [11]. In the present study, the radial compression of C_{60}, $C_{60}F_{60}$ and $C_{60}H_{60}$ molecules was simulated, and their electronic structures during the compression were calculated using the semi-empirical quantum molecular dynamics (QMD) method [2]. The mechanical properties and chemical stability of the three molecules under compression are discussed.

This paper reveals the mechanical properties and electronic structure changes of the C_{60}, $C_{60}H_{60}$ and $C_{60}F_{60}$ molecules under compression, and some correlative results are very helpful for researchers to recognise the properties of the molecular bearing balls.

2. Model and method

In this paper, the molecular bearing balls of C_{60}, $C_{60}F_{60}$ and $C_{60}H_{60}$ are chosen as objects to be investigated. These spherical molecules, geometrically optimised by the parametric method 3 (PM3) [12] and the semi-empirical quantum mechanics (QM) method, are shown in Figure 1, respectively. Their molecular weight W_0, diameter h_0, volume V_0 and energy E_0, as well as their C—C, C—H and C—F bond length, are listed in Table 1.

The QMD technique [2] is used to simulate radial compressions of the spherical molecules. In the QMD simulations, the compressive deformation of the three molecules are implemented by changing the distance h between two atoms farthest away from each other in the spherical molecules. The steps of the simulations can be described as follows: firstly, changing the distance h between two atoms farthest away from each other in the spherical molecules from the initial distance h_0, namely the initial diameter of the molecules; secondly, 'fixing' the

*Email: shj@nuaa.edu.cn

ISSN 0892-7022 print/ISSN 1029-0435 online

DOI: 10.1080/08927020802430737
http://www.informaworld.com

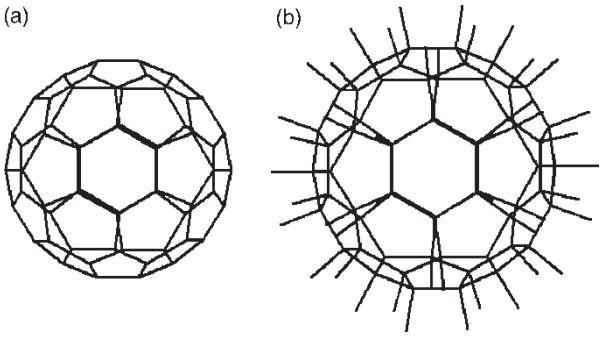

Figure 1. The molecular bearing balls of (a) C_{60}, (b) $C_{60}F_{60}$ or $C_{60}H_{60}$.

two atoms and then 'relaxing' the other atoms by the QMD method, and in the end of the relaxation obtaining the molecular energy E corresponding to the given compressive strain $l = |h - h_0|/h_0$; thirdly, repeating the above two steps to obtain a series of E data corresponding to a different strain l; finally, analysing the E–l data to obtain the molecular energy E and loading F during the compressions.

In the QMD technique, the positions and velocities of the C, H and F atoms are predicted with Newton's equation:

$$\ddot{r}_i = F_i(r_i)/m_i, \tag{1}$$

$$F_i = -\frac{\partial E}{\partial r_i}, \tag{2}$$

where $\ddot{r}_i$, F_i and m_i are the acceleration, the resultant force and the mass of the ith C, H or F atom, respectively, and r_i is the dimensional coordinates of the ith atom, and the molecular energy E is determined by solving the following Schrödinger equation:

$$\mathbf{H}\Psi = E\Psi, \tag{3}$$

where $\mathbf{H}$ is the Hamilton operator and Ψ is the wave function of the investigated molecular system.

In fact, for large molecular systems, it is very difficult to accurately solve the above Schrödinger equation. However, in accordance to the Born–Oppenheimer assumption that electronic motions can be decoupled from those of nuclei, and the Hartree–Fock assumption, the polyelectronic problem in Equation (3) is translated into a single electronic problem. The simplified single electronic problem can be expressed by the following Hartree–Fock equation:

$$\mathbf{H}_i\Psi_i = \varepsilon_i\Psi_i, \tag{4}$$

where $\mathbf{H}_i$ is the effective Hamilton operator, Ψ_i is the ith molecular orbital (MO) and ε_i is the energy corresponding to the MO Ψ_i.

According to the assumption of linear combination of atomic orbitals, Ψ_i can be expressed as

$$\Psi_i = \sum_{\mu} C_{\mu_i}\Phi_\mu, \tag{5}$$

where Φ_μ is the μth atomic orbital (AO) and $C_{\mu i}$ is the coefficient of the AO Φ_μ.

Adopting the close-shell model and the restricted Hartree–Fock method [13], Formula (4) can be translated into the following matrix form [14]:

$$\mathbf{FC} = \mathbf{SCE}, \tag{6}$$

where $\mathbf{F}$ is the Fock matrix, $\mathbf{S}$ is the overlapping matrix, $\mathbf{C}$ is the coefficient matrix and $\mathbf{E}$ is the diagonal matrix of energy.

The total electronic energy of the molecular system is obtained by solving Equation (6), which adopts the self-consistent field (SCF) approach, and the total energy E of the system is further obtained with the electronic energy plus the interaction between nuclei.

In the present QMD simulations, the PM3 [12] semi-empirical QM method is employed to improve the efficiency. All the mechanisms, which include modelling C_{60}, $C_{60}F_{60}$ and $C_{60}H_{60}$, compressing the molecules and relaxing the C, H or F atoms by the QMD method, are carried out by the famous quantum chemical software HyperChem 7®. The time step of 0.0005 ps for the MD simulation and the convergence limit of 0.042 KJ/mol for the SCF QM simulation are taken into consideration.

Table 1. The geometrical, physical and mechanical parameters for C_{60}, $C_{60}F_{60}$ and $C_{60}H_{60}$ molecules.

Molecules	C_{60}	$C_{60}F_{60}$	$C_{60}H_{60}$
W_0	720	1860	780
h_0 (Å)	7.14	10.59	9.78
V_0 (Å^3)	190.49	621.54	489.55
E_0 (KJ/mol)	−2854062	−13495260	−3233146
Bond length (Å)			
C—C	1.39	1.57	1.51
C—H or C—F	–	1.38	1.12
F_{max} (nN)	1.42	3.03	1.71
l_i (%)	20.4	21.0	20.8

3. Results and discussion

3.1 Compressive properties of C_{60}, $C_{60}F_{60}$ and $C_{60}H_{60}$

Figures 2–4 present the configuration evolvement of the compressed C_{60}, $C_{60}F_{60}$ and $C_{60}H_{60}$. In Figures 2–4, the arrowheads are used to mark the locations of the 'fixed' atoms. Figure 5 presents the relationship between the molecular energy increment $\Delta E = E - E_0$ and the strain l for the three molecules.

Because the molecular energy increment ΔE mainly comes from the mechanical work of the external loading

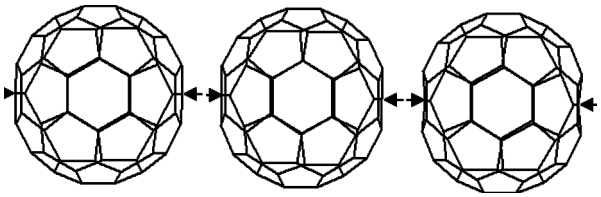

Figure 2. The compressed C_{60}. (a) $l = 12\%$, (b) $l = 18\%$ and (c) $l = 24\%$.

F, the relationship between the compressive loading F and the strain l for the molecules can be deduced from Figure 5 by differentiation with respect to strain. The obtained F–l curves of C_{60}, $C_{60}F_{60}$ and $C_{60}H_{60}$ are presented in Figure 6.

From Figures 2–6, the following findings are obtained:

(1) When the strain l increases to certain values, the compressed spherical molecules will 'cave in' at the locations of the two 'fixed' and 'loaded' atoms (Figures 2(c), 3(c) and 4(c)).
(2) The molecular energy E for all the compressed fullerenes increases monotonously with the strain l. Under the same strain l, the ΔE of the three molecules has the order of $C_{60}F_{60} > C_{60}H_{60} > C_{60}$, which implies that $C_{60}F_{60}$ has the best energy-absorbing capability and C_{60} the worst one.
(3) The compressive loading F increases gradually with the strain l up to the values l_i, and after that the spherical molecules cave in, and their compressive loading F decreases with the increase of the strain l, where the maximal loading F_{max} are called as 'endurance limit' and the corresponding strain l_i are defined as 'failure strain' (Figure 6). The F_{max} and l_i values are listed in Table 1.
(4) The F_{max} and l_i can be used to characterise the load and deformation support capabilities of material, respectively; generally, the higher the F_{max} and l_i values are, the better its load and deformation support capabilities are [15]. Apparently, the present $C_{60}F_{60}$ has the best load support capability and C_{60} the worst one, but their deformation support capability seems to be comparable.

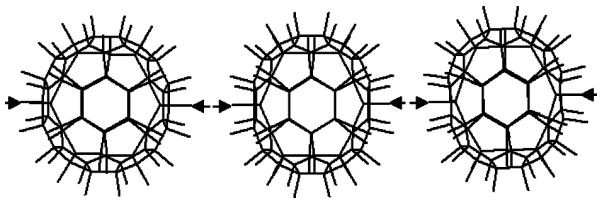

Figure 3. The compressed $C_{60}F_{60}$. (a) $l = 12\%$, (b) $l = 18\%$ and (c) $l = 24\%$.

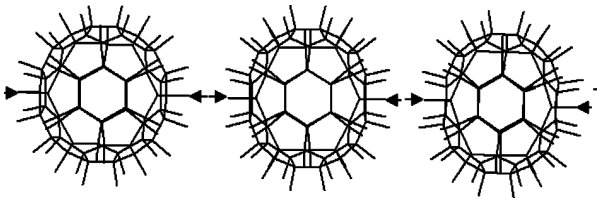

Figure 4. The compressed $C_{60}H_{60}$. (a)$l = 12\%$, (b) $l = 18\%$ and (c) $l = 24\%$.

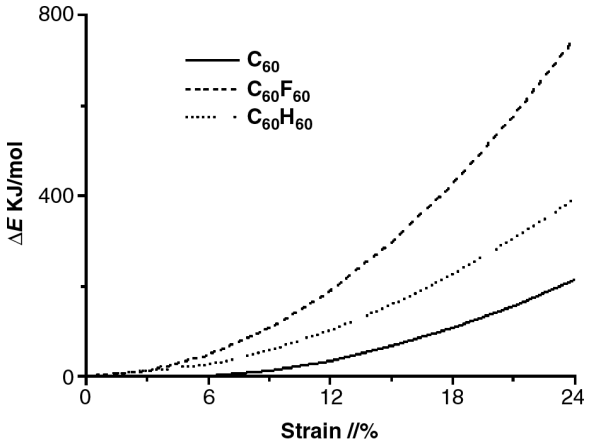

Figure 5. The correlation of molecular energy increment ΔE to strain l for the compressed C_{60}, $C_{60}F_{60}$ and $C_{60}H_{60}$.

In [16], Brenner's reactive empirical bond-order potential [17,18]-based molecular dynamics (MD) method is adopted to simulate the compression of C_{60}. It is found that the compressed C_{60} begins to cave in at $l \approx 25\%$, corresponding to the external load $F \approx 0.98$nN. The present F_{max} and l_i values of C_{60}, i.e. 1.42 nN and 20.4%,

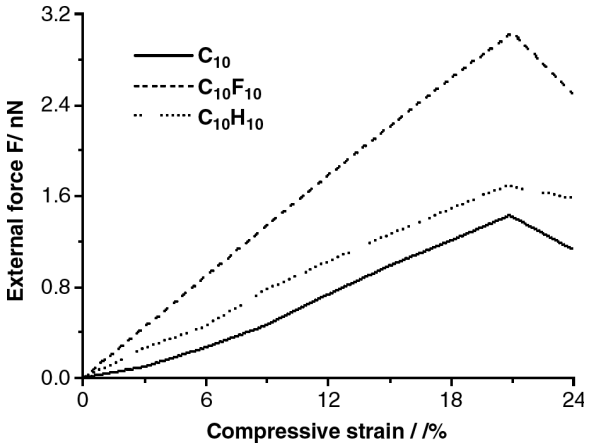

Figure 6. The correlation of compressive loading F to strain l for the compressed C_{60}, $C_{60}F_{60}$ and $C_{60}H_{60}$.

are close to the ones in [16], respectively, which implies the validity of the present calculations.

In [19], we also adopted the Tersoff potential-based MD method to simulate the compression of C_{60} under two parallel graphite layers. It is found that the compressed C_{60} has $F_{ma} \approx$ 21nN and $l_i \approx 27\%$. The F_{ma} and l_i values are much larger than the results in the present paper, respectively. What causes the differences? It can be explained by the difference in the loading styles. Differing from the present point loading, in [19], two rigid graphite layers were used to compress C_{60}, which implies that graphite layers and C_{60} have a larger loaded area, hence C_{60} under rigid graphite layers has a larger endurance limit and failure strain.

3.2 Electronic structures of C_{60}, $C_{60}F_{60}$ and $C_{60}H_{60}$ under compression

According to the FMO theory [20,21], it is considered that the FMOs, i.e. the molecular orbitals (MOs) near the LUMO and HOMO, determine the chemical properties of one molecule. The LUMO and HOMO energy can reflect molecular electrophilicity and nucleophilicity, respectively. The LUMO energy is close to the molecular electrophilic potential in value, and the higher the HOMO energy is, the easier the molecule loses its electron. The energy gap between the LUMO and HOMO can reflect the capability of electron transferring from the occupied MO to the unoccupied one. Therefore, in the present paper, the FMO energy and the LUMO–HOMO energy gap for the compressed molecules are mainly discussed.

By the QMD calculations, Figures 7–9 present the changes in the FMO energy levels for the three molecules during compression. In Figures 7–9, for clarity, the short horizontal lines are used to mark the unoccupied MOs and the long ones the occupied MOs. Figure 10 presents the changes in the HOMO and LUMO energy as well as the LUMO–HOMO energy gap for the compressed C_{60}, $C_{60}F_{60}$ and $C_{60}H_{60}$ molecules.

From Figures 7–10, the following findings are obtained:

(1) The LUMO, HOMO energy and the LUMO–HOMO energy gap for the undeformed C_{60} molecule are -3.09, -9.41 and 6.33 eV, those of the undeformed $C_{60}F_{60}$ molecule are -3.08, -15.61 and 12.52 eV and those of the $C_{60}H_{60}$ molecule are 3.10, -10.03 and 13.13 eV, respectively. Both the $C_{60}F_{60}$ and $C_{60}H_{60}$ molecules have lower HOMO energy, higher LUMO energy and wider LUMO–HOMO energy gap than C_{60}, which denote that the C_{60} molecule easily loses electron and has worse chemical stability than two other fuzzy balls.

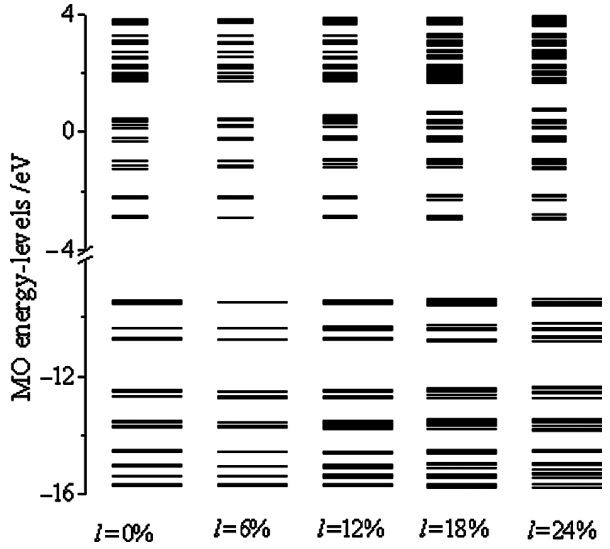

Figure 7. The FMO energy levels of C_{60} under compression.

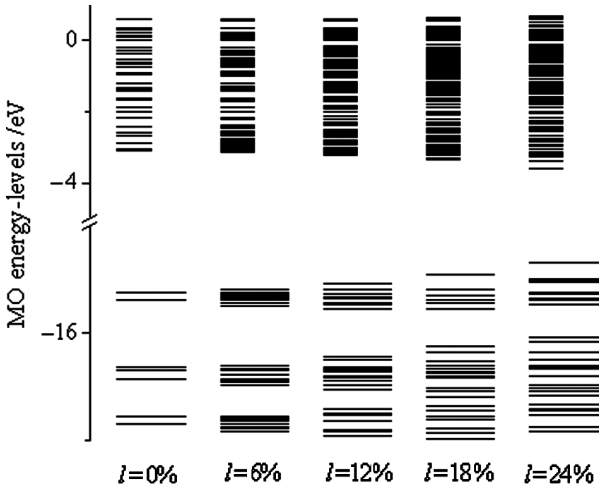

Figure 8. The FMO energy levels of $C_{60}F_{60}$ under compression.

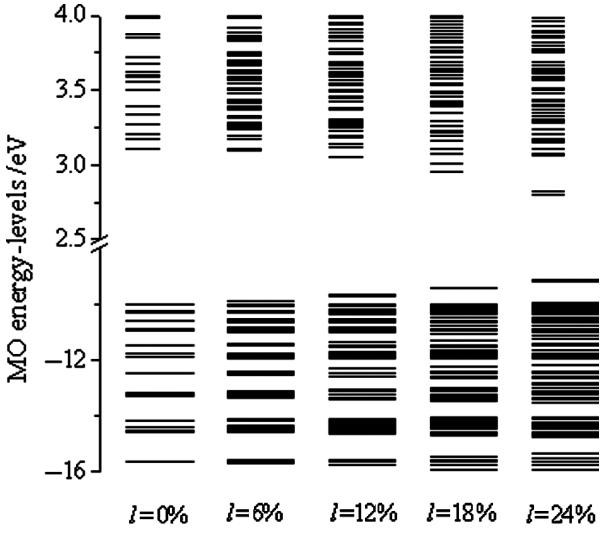

Figure 9. The FMO energy levels of $C_{60}H_{60}$ under compression.

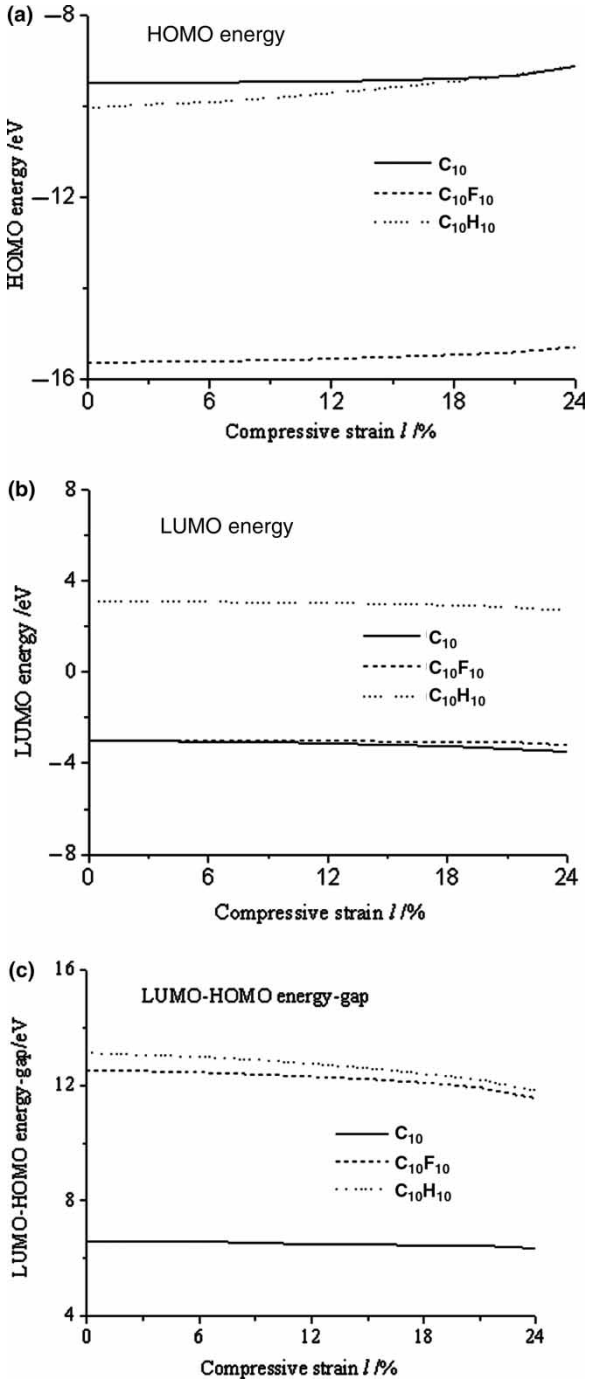

Figure 10. The changes of (a) HOMO, (b) LUMO energy and (c) LUMO–HOMO energy gap.

(2) With the increase of compressive strain, the LUMO energy and LUMO–HOMO energy gap of the three molecules decrease, but their HOMO energy increases, which implies that the compressed C_{60}, $C_{60}F_{60}$ and $C_{60}H_{60}$ molecules have lower excitation energy of HOMO electron(s) and become more chemically active.

(3) Under the same compressive strain, the $C_{60}F_{60}$ and $C_{60}H_{60}$ molecules have lower HOMO energy, as well as higher LUMO energy and wider LUMO–HOMO energy gap, which implies that the compressed $C_{60}F_{60}$ and $C_{60}H_{60}$ have better chemical stability than the compressed C_{60} all the time.

(4) Due to the configuration change, the MO energy levels of the compressed molecular bearing balls change, and especially after the compressed molecules cave in at the loading positions, i.e. after $l \approx 21\%$, their LUMO–HOMO energy gaps decrease markedly. This denotes that after the 'caving in' the compressed molecular bearing balls will markedly become chemically active.

4. Conclusions

The QMD simulations of the C_{60}, $C_{60}F_{60}$ and $C_{60}H_{60}$ molecules under compression are run to investigate their mechanical properties and electronic structures. Based on this, the following conclusions were drawn:

(1) The $C_{60}F_{60}$ and $C_{60}H_{60}$ molecules have better load support and energy-absorbing capabilities than the C_{60} molecule, but their deformation support capability is comparable.

(2) The compressed molecules will become more chemically active, but under the same compressive strain, the $C_{60}F_{60}$ and $C_{60}H_{60}$ molecules have better chemical stability than the C_{60} molecule.

References

[1] H.W. Kroto, J.R. Heath, S.C. Brien, R.F. Curl, and R.E. Smalley, *C_{60}: buckminsterfullerene*, Nature 318 (1985), pp. 162–163.
[2] H. Shen, *Geometrical deformation and failure behavior of C_{60} diamer under applied external electric field*, Mol. Simul. 32(1) (2006), pp. 59–64.
[3] B. Climen, B. Concina, M.A. Lebeault, F. Lépine, B. Baguenard, and C. Bordas, *Ion-imaging study of C_{60} fragmentation*, Chem. Phys. Lett. 437 (2007), pp. 17–22.
[4] T. Coffey and J. Krim, *C_{60} molecular bearings and the phenomenon of nanomapping*, Phys. Rev. Lett. 96 (2006), 186104.
[5] H. Shen, *MD simulations of polymeric C_{60} fullerene layers/chain under tension*, Mol. Simul. 32(5) (2006), pp. 385–390.
[6] S. Kawasaki, F. Okino, and H. Touhara, *Discrete-variational X_α calculations of $C_{60}F_x$ with $x = 0$, 36, and 48*, Phys. Rev. B 24(53) (1996), pp. 16652–16655.
[7] Z. Wu, X. Deng, Y. Lin, D. Cheng, and M. Zhan, *Synthesis and photoelectric property for the fullerene complex $C_{60}(Ph_2PCH_2CH_2CH_2CH_2PPh_2)$*, Chin. J. Inorg. Chem. 22(2) (2006), pp. 217–229.
[8] C. Jerzy, *Electronic structures of the icosahedral $C_{60}H_{60}$ and $C_{60}F_{60}$ molecules*, Chem. Phys. Lett. 181(1) (1991), pp. 68–72.
[9] J. Groß, G. Harder, F. Vögtle, H. Stephan, and K. Gloe, *$C_{60}H_{60}$ und $C_{54}H_{48}$: extraction through silver-ion and new concave hydrocarbon*, Angew. Chem. 107(4) (2006), pp. 523–526.
[10] D.V. Massimiliano, E. Stephane, and R.H. James, *Introduction to Nanoscale Science and Technology*, Kluwer Academic Publishers, Dordrecht, 2004, p. 132.
[11] H. Shen, *Tensile properties and electronic structures of C_{240} nanotube and 4C_{60} fullerene polymers*, Int. J. Nanosci. 4(2) (2006), pp. 99–108.

[12] J. Stewart, *Optimization of parameters for semi-empirical methods. I. Method*, J. Comput. Chem. 10 (1989), pp. 209–220.
[13] J. Collins, P. Schleyer, J. Binkley, and J. Pople, *Self-consistent molecular orbital methods. XVII. Geometries and binding energies of second-row molecules. A comparison of three basis sets*, J. Chem. Phys. 64 (1976), pp. 5142–5151.
[14] A.R. Leach, *Molecular Modeling*, Addison Wesley Longman Limited, Toronto, 1996, pp. 316–317.
[15] H. Shen, *Compressive and tensile mechanical properties of Ar-filled carbon nanopeapods*, Mater. Lett. 61(2) (2007), pp. 527–530.
[16] H. Shen, *Mechanical properties and electronic structure of compressed C_{60},C_{180} and C_{60}@C_{180} fullerenes*, J. Mater. Sci. 42 (2007), pp. 7337–7342.
[17] D.H. Robertson, D.W. Brenner, and C.T. White, *On the way to fullerenes: molecular dynamics study of the curling of graphitic ribbons*, J. Phys. Chem. 96 (1992), pp. 6133–6135.
[18] R.C. Mowrey, D.W. Brenner, B.I. Dunlap, J.W. Mintmire, and C.T. White, *Simulations of buckminster fullerene C_{60} collisions with a hydrogen-terminated diamond {111} surface*, J. Phys. Chem. 95 (1991), pp. 7138–7142.
[19] H. Shen and X. Mu, *Compressive mechanical properties of C_{60},C_{240} and C_{60}@C_{240} fullerenes*, J. Atom. Mol. Phys. 23(5) (2006), pp. 850–854.
[20] Q. Yu and L. Zhu, *Introduction into Molecular Design*, Higher Education Press, Beijing, 1998, p. 67.
[21] I. Fleming, *Frontier Orbitals and Organic Chemical Reactions*, Wiley Publisher, Indianapolis, 2003, p. 56.